J Nanopart Res (2016) 18:35
DOI 10.1007/s11051-016-3343-z

RESEARCH PAPER

Deposition of conductive TiN shells on SiO_2 nanoparticles with a fluidized bed ALD reactor

Arjen Didden · Philipp Hillebrand · Markus Wollgarten · Bernard Dam · Roel van de Krol

Abstract Conductive TiN shells have been deposited on SiO_2 nanoparticles (10–20 nm primary particle size) with fluidized bed atomic layer deposition using TDMAT and NH_3 as precursors. Analysis of the powders confirms that shell growth saturates at approximately 0.4 nm/cycle at TDMAT doses of >1.2 mmol/g of powder. TEM and XPS analysis showed that all particles were coated with homogeneous shells containing titanium. Due to the large specific surface area of the nanoparticles, the TiN shells rapidly oxidize upon exposure to air. Electrical measurements show that the partially oxidized shells are conducting, with apparent resistivity of approximately $\sim$11 kΩ cm. The resistivity of the powders is strongly influenced by the NH_3 dose, with a smaller dose giving an order-of-magnitude higher resistivity.

Keywords Fluidized bed · Atomic layer deposition · Core–shell particles · Titanium nitride · Conductive shells · Microelectronic contacts

A. Didden · B. Dam · R. van de Krol (✉)
Faculty of Applied Sciences, Materials for Energy Conversion and Storage, Delft University of Technology, P.O. Box 5045, 2600 GA Delft, The Netherlands
e-mail: roel.vandekrol@helmholtz-berlin.de

P. Hillebrand · M. Wollgarten · R. van de Krol
Helmholtz-Zentrum Berlin für Materialien und Energie GmbH, Institute for Solar Fuels, Hahn-Meitner-Platz 1, 14109 Berlin, Germany

Introduction

Nanoparticles and nanoparticle assemblies are the cornerstones of current material science and engineering. The nanometer size and structure provide properties and functionalities that make the particles interesting for a wide variety of potential applications such as microelectronics, solar energy conversion, sensors, catalysis, and batteries. Much research is being done on the synthesis of core–shell materials, in which the core and the shell are made of different materials and have different functionalities. For example, the shells can be used for corrosion protection (Amarnath et al. 2013; Khurshid et al. 2013; Ma et al. 2010; Magdassi et al. 2010) or improved catalytic performance, (Tedsree et al. 2011; Zhang et al. 2012) whereas the bulk can be used as optical absorption center, (Ma et al. 2010) intercalation material for charge storage, (Ren et al. 2008) or inert support material.

When used in microelectronic devices, a low resistivity of the nanoparticle assemblies and the ability to fabricate good electrical contacts to the nanoparticles are crucial for proper functioning. This can be very challenging to achieve. One solution is to coat the nanoparticles with a thin, electrically conducting layer using fluidized bed atomic layer deposition (FB-ALD). This technique, developed by Wank et al. (2004), combines the wide range of materials that can be deposited with ALD with the ability to coat large amounts of nanoparticles without having the

Published online: 08 February 2016

diffusional limitations of ALD coatings in fixed beds (Longrie et al. 2014a) and the scalability provided by fluidized bed reactors (van Ommen et al. 2010). ALD offers the possibility to grow ultra-thin coatings of a wide variety of materials in a controlled, atomic layer-by-atomic layer fashion. Earlier research by Hakim et al. shows that with this technique, through the process of dynamic aggregation of nanoparticle agglomerates, it is possible to coat individual nanoparticles with homogeneous layers (Hakim et al. 2005a, b, c).

In this paper, we report on the ALD of conductive TiN shells on non-conducting SiO_2 nanoparticles with a fluidized bed reactor. TiN is a low-cost material that is, e.g., used as diffusion barrier for Cu or Al in silicon-based microelectronics and can be deposited at the relatively low temperatures required for nanoparticle processing by metal–organic ALD. Due to its conductivity, TiN also shows enhanced surface plasmon effects (Cortie et al. 2010) that can be useful in applications such as sensors and photocatalysis (Boriskina et al. 2013). Furthermore, TiN coatings, deposited with conventional ALD have been reported to improve the performance of batteries made with lithium titanate spinel nanoparticles (Snyder et al. 2007).

We have deposited the material with a low-temperature process using tetrakis (dimethylamino-) titanium (TDMAT) and NH_3 as precursors. This chemistry was chosen over the more common $TiCl_4$ deposition process because of the large amounts of by-products that are formed due to the large specific surface area of the powder. When $TiCl_4$ is used, large amounts of highly corrosive HCl are formed that can damage downstream equipment. Furthermore, the use of TDMAT also avoids contamination of the powder with NH_4Cl, which is known to form in $TiCl_4$-based processes (Elers et al. 2002). Thermal ALD was used rather than plasma-enhanced ALD, even though PE-ALD should give superior coating quality on nanoparticles (Longrie et al. 2014b), because it allows for a less complicated reactor design that is more easily scaled up.

We will show that the chosen chemistry and reactor design results in self-limiting growth of the TiN shells. Although the TiN layers almost completely oxidize after prolonged exposure to air, we find that the SiO_2–TiN particle network is electrically conducting. These results represent a step forward in highly controlled gas-phase deposition of electrically conducting shells on powder-based nanoparticles.

Experimental

TiN coatings were deposited on SiO_2 nanoparticles with a specific surface area of 90 m^2/g and an average diameter of $\sim$25 nm (Aerosil 90, Evonik) using the fluidized bed ALD reactor described elsewhere (Didden et al. 2014). Before deposition, the minimum fluidization velocity was determined by measuring the pressure drop at different Ar flow rates. TDMAT (SAFC hitech, electronic grade) and dried, gaseous NH_3 (Linde gas, grade 3.8) were used as precursors. NH_3 is dried by leading it through a CaO absorption bed to prevent oxidation of the TiN films by water present in the gas. TDMAT was admitted to the reactor by bubbling 1 sccm (standard cubic centimeter per minute) of Ar through the bubbler. The bubbler temperature was 80 °C to ensure sufficient vapor pressure, and the precursor supply lines were kept at 90 °C to prevent condensation. A constant additional flow of Ar (1.5 sccm) was fed into the reactor to assist in the fluidization of the particles. The ammonia was delivered by a mass flow controller with a flow range of 0–3 sccm that was equipped with NH_3-resistant Buna-N seals. The reactor was operated at 150 °C and 0.5 mbar. The temperature was selected in such a way that, according to the literature on TDMAT–NH_3 processes,(Elam et al. 2003; Fillot et al. 2005; Miikkulainen et al. 2013; Musschoot et al. 2009) high growth rates could be obtained without running the risk of TDMAT decomposition in the gas phase and concomitant unsaturated film growth.

The ALD reaction scheme of the TDMAT pulse → purge → NH_3 pulse → Purge cycles is given in Table 1. The number of cycles determines the layer thickness. After the last cycle (ending with a NH_3 pulse), a prolonged purge step was used to ensure that the reactor was completely free of TDMAT and NH_3 before being opened to recover the particles.

The Ti content of the powder was determined by first completely oxidizing the TiN to TiO_2 by annealing it at 250 °C in air for 6 h and then dissolving the TiO_2 in hot sulfuric acid before measuring the concentration of dissolved Ti with the UV/Vis method described elsewhere (Didden et al. 2014). The core–shell structure was investigated in a transmission

Table 1 Process scheme of FB-ALD reaction

Reaction step	TDMAT pulse	Purge	NH_3 pulse	Purge
Time	600–1800 s	300 s	300 s	300 s
Ar flow	2.5 sccm	2.5 sccm	2.5 sccm	2.5 sccm
TDMAT flow	~0.45 sccm[a]	0	0	0
NH_3 flow	0 sccm	0 sccm	1–3 sccm	0 sccm

[a] Estimated value, calculated by the method described elsewhere (Didden et al. 2014)

electron microscope (TEM, Zeiss Libra 200FE) equipped with an Omega-type energy filter. Zero-loss filtered images as well as elemental maps were acquired (Heil and Kohl 2010) using the Ti-$L_{2,3}$, N-K, and O-K edge, respectively.

X-ray photoelectron spectroscopy (XPS) measurements were carried out with a Specs XR50 X-ray source (Mg Kα radiation) and a Phoibos 100 analyzer.

The conductivity of the powder was assessed by pressing a small amount of powder between two plates of conductive glass (F-doped SnO_2, TEC-15, 15 Ohm/square, Hartford Glass Co.) after which the resistance was measured with a digital multimeter (Keithley model 2001). The electrode area was 45 mm^2 and the distance between the plates 50 µm. Control experiments were done with uncoated Aerosil 90, pure TiN powder (Sigma Aldrich, <3 µm particle size), and pure TiO_2 (Aeroxide P25, Evonik).

Results and discussion

Oxidation of TiN shell

After the deposition process, the powders have a very dark green–brown color that is similar to that of fine TiN powder. When opening the reactor after the deposition, the powder rapidly changed to a light-brown color upon contact with air. As thin porous TiN films are known to oxidize at the grain boundaries when brought into contact with air, (Elam et al. 2003; Logothetidis et al. 1999; Zhao et al. 2000) this is most likely due to oxidation of the TiN to TiO_xN_y. The latter phase indeed has a light-brown to yellow color.

The fast oxidation of ALD-TiN in air means that special care has to be taken when removing the TiN-coated SiO_2 particles from the reactor. During the first test experiments, the nanoparticles burn red hot when opening the reactor too quickly. The result was a sintered piece of nanoparticle material. The temperature increase is attributed to the large amount of heat produced during the oxidation reaction: $TiN + O_2 \rightarrow TiO_2 + \frac{1}{2}N_2$ ($\Delta G^0 = -581$ kJ/mol, $\Delta H = -607$ kJ/mol). To illustrate how oxidation of a relatively thin shell of a nanopowder can indeed cause significant heating, we consider a batch of 0.5 gram SiO_2 powder. With a heat capacity of 0.75 J/(gK) for SiO_2, (Hayes and Lide 2015) the total energy required to heat this batch of powder from room temperature (25 °C) to 700 °C is 253 J. This energy can be provided by oxidizing 26 mg of TiN–TiO_2, which corresponds to 5.2 % of the total mass of the powder. This translates to a ~0.4 nm TiN shell around a 90-nm diameter SiO_2 particle, assuming both materials are fully dense. This surprisingly small number clearly shows that even incomplete oxidation of a thin TiN shell can generate enough heat to let the powder become red hot upon exposure to air (especially when the reaction accelerates itself due to thermal runaway).

To slow down the oxidation reaction, we filled the reactor very slowly with air. Opening the reactor slowly does not completely prevent the oxidation, but it slows down the reaction rate and thus prevents the powder from burning and sintering.

Film growth rate

If film growth occurs in the self-limiting growth regime that is characteristic for ALD, the TiN layer thickness should be independent from the TDMAT dose. To verify this, batches of 0.5 g powder were coated with 50 ALD cycles using different TDMAT dosages while keeping the NH_3 dose constant. The TDMAT flow is calculated from the Ar flow, the pressure in the precursor bubbler, and the saturated

vapor pressure of TDMAT, with the method described previously (Didden et al. 2014). The base gas flow rate used for fluidization was 2.5 sccm, and this did not include the additional gas flow due to the precursor doses. The gas flow rate was thus well above the measured minimum fluidization flow rate of 1.5 sccm determined by measuring the gas flow at which the pressure drop remains constant (see Fig. 1).

The concentration of TiN is calculated from the total amount Ti in the powder as measured by UV–Vis. The data presented in Fig. 2 show that the growth of TiN saturates at TDMAT doses >1.2 mmol/g/cycle, indicating that we indeed operate in the self-limiting growth regime.

The growth per cycle (GPC) can be estimated from the mass fraction x by using the equation:

$$\mathrm{GPC} = \frac{d_0}{2N}\left(\sqrt[3]{\frac{x}{1-x}\frac{\rho_{SiO_2}}{\rho_{\mathrm{TiN}}}+1}-1\right). \quad (1)$$

In this equation, d_0 is the primary particle diameter (nm), N the number of cycles, and ρ_{SiO2} and ρ_{TiN} the density of SiO_2 and TiN, respectively. The derivation of this equation can be found in the appendix. The density of amorphous SiO_2 is 2.65 g/cm^3, (Hayes and Lide 2015), whereas for the density of ALD-TiN, an estimated value of 3.0 g/cm^3 (as reported in literature for thermal TDMAT-NH_3 deposition processes) (Fillot et al. 2005; Miikkulainen et al. 2013) was used. The estimated primary particle size, based on a specific surface area of 90 m^2/g and a density of 2.65 g/cm^3, is

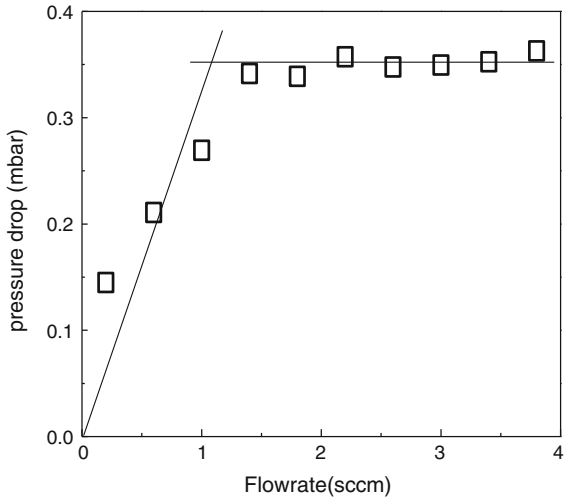

Fig. 1 Pressure drop as a function of the Ar flow. The crossing point of the lines indicates the minimum fluidization velocity

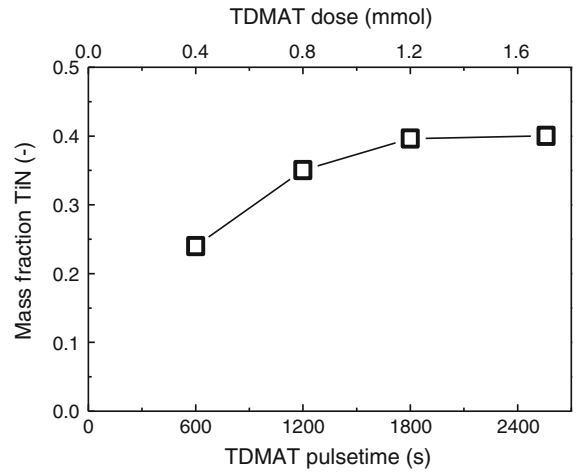

Fig. 2 Concentration of TiN on particles in relation to the TDMAT dose. The mass fractions were measured after 50 ALD cycles for all datapoints. The NH_3 pulse time was 300 s at a flow rate of 1 sccm. The reactor was operated at 150 °C and 0.5 mbar

25 nm. With this particle diameter, the GPC is equal to approximately 0.4 Å/cycle. This value is in the lower range of the 0.4–1.2 Å/cycle growth rates reported in the literature for thermal TDMAT/NH_3 ALD processes (Elam et al. 2003; Fillot et al. 2005; Musschoot et al. 2009).

The efficiency of precursor use is calculated by comparing the precursor dose per gram to the mass fraction of TiN. The mass fraction is 0.4, which means that the total amount of TiN deposited is 5 mmol, and the deposition efficiency of TDMAT is approximately 16.7 %. For NH_3, the efficiency is much higher, roughly 50 % of the nitrogen atoms admitted into the reactor as NH_3 ends up in the film. This is much lower than the near 100 % efficiency that one would normally expect for fluidized bed ALD processes (King et al. 2007).

Possible explanations for the lower GPC and efficiency are growth inhibition in the first deposition cycles, or incomplete coverage of the particles due to clustering of the nanoparticles (agglomeration). Growth inhibition may occur, but since the GPC actually *decreases* after 20 cycles (vide infra), it seems unlikely that this can explain the low deposition efficiencies. Agglomeration would lead to some particles being blocked from contact with the gas. While we cannot rule this out completely, we found no indication whatsoever of partially coated particles in our TEM analysis (vide infra). This is consistent with

the process of dynamic aggregation as described by Hakim et al., suggestion that our SiO_2 powders only form so-called 'soft aggregates' that can be broken up by the fluidization process (Hakim et al. 2005a, b, c).

Another possible cause for the low efficiency is the presence of inhomogeneities in the fluidized bed, which would reduce the mass transfer rate between the gas phase and the particle surface. In a homogenously fluidized bed, mass transfer is usually not rate limiting because the residence time of the gas is orders of magnitude longer than the time scale at which mass transfer takes place. The presence of large gas bubbles and channeling effects can, however, lead to poor mass transfer between gas phase and particle surface and, hence, poor precursor efficiency (Grillo et al. 2015). Although we cannot rule this out, visual inspection of the bed and the data in Fig. 1 did not give any indication of inhomogeneous fluidization.

Besides agglomeration and bed inhomogeneities, there is a growth limitation that is inherent to the TDMAT process. Dimethylamine—a by-product of the deposition reaction—is known to adsorb strongly on TiN surfaces and in such a way block TDMAT absorption sites. (Okada and George 1999) Due to the intimate contact between the gas phase and the particles, this effect is more strongly present in fluidized bed ALD reactors than in conventional ALD reactors. The difference between the processes is depicted in Fig. 3. In conventional ALD (on fixed substrates), re-adsorption of dimethylamine is usually not a major issue because, as soon as the DMA molecules are released from the surface; they are quickly transported to the reactor exit by the feed gas and do not get a chance to re-adsorb to the substrate. However, in a fluidized bed reactor, a dimethylamine molecule will have to pass many particles on its way to the exit, dramatically increasing the chance to re-adsorb on a particle surface. While the increased chance of (re-)adsorption of precursor molecules is the reason that precursor efficiency is usually extremely high in fluidized bed reactors, we believe that the re-adsorption of reaction by-products which block the adsorption sites is the reason that the GPC and the precursor efficiency are rather low for the TDMAT–NH_3 FB–ALD process.

Knowing the saturated growth rate to be 0.4 Å/cycle, the next step is to determine whether this growth rate remains constant with increasing number of cycles. To investigate this, batches with identical TDMAT and NH_3 doses (1200 and 300 s pulses, respectively) but with different number of ALD cycles have been prepared. The data presented in Fig. 4 (red squares) show that the TiN mass fraction increases with increasing amount of cycles. The growth rate, however, strongly decreases after depositing 50 cycles, as indicated by the black circles in Fig. 4.

The decreasing average growth rates could indicate that growth enhancement rather than growth inhibition

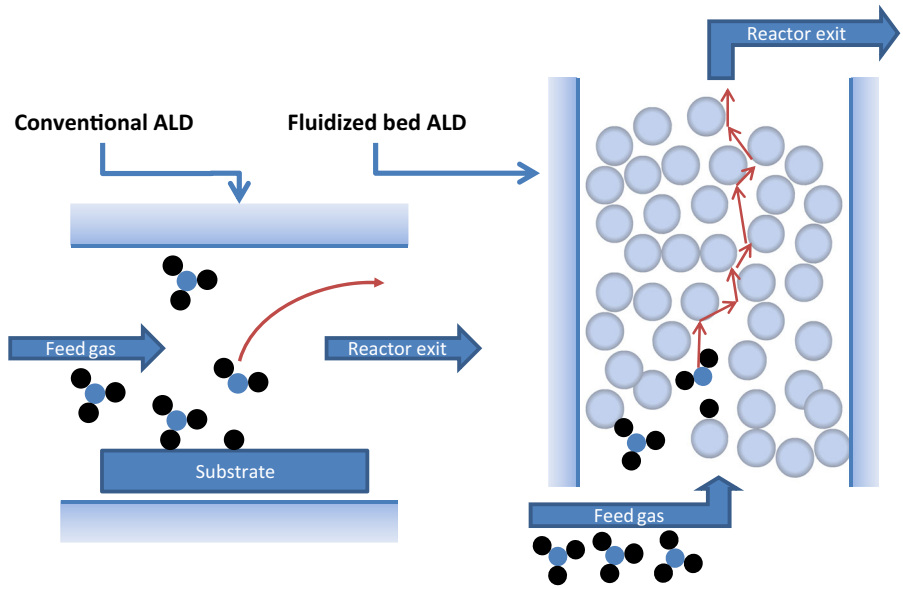

Fig. 3 Removal of a DMA molecule by sweep gas in a "conventional" ALD reactor with a single substrate and a fluidized bed ALD reactor filled with particles. Once a TDMAT molecule has attached to the substrate surface, the released DMA molecule has to travel through the reactor to the exit

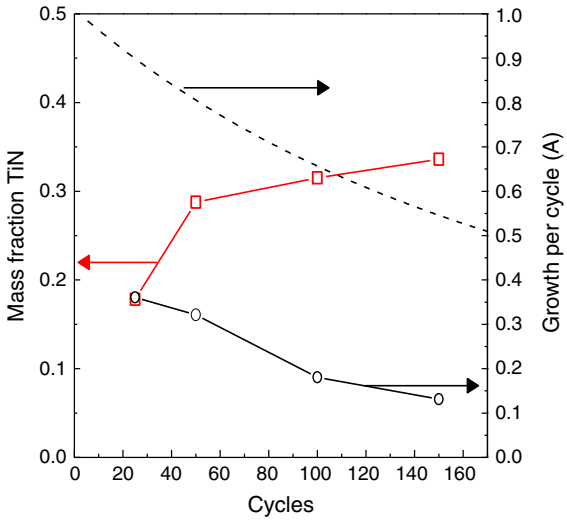

Fig. 4 TiN mass fraction (*squares*) and growth per cycle (*circles*) with constant 1200 s TDMAT and 300 s NH_3 dose. (The *lines* serve as a guide to the eye). The maximum achievable growth rate per cycle as calculated from the TDMAT and NH_3 doses is indicated by the *dashed line*. (Color figure online)

is occurring during the first cycles. This phenomenon has been reported before for TiN-ALD ALD on Si wafers with TDMAT and NH_3 as precursors (Musschoot et al. 2009).

Another explanation could be underexposure to either TDMAT or NH_3. To illustrate this, assume that the respective exposures of TDMAT and NH_3 are x and y mol per cycle, and that $x < y$. Then, a maximum TiN deposition rate of x mol per cycle can be achieved. During cycle n, the total amount of TiN per cycle x has to be deposited on a surface area A_{n_1}, causing an increase in particle diameter and, concomitantly, surface area. Assuming that the increase in particle diameter is much smaller than the particle size, the surface area of the particles after cycle n can be estimated with the equation:

$$A_{\mathrm{n}} = A_{\mathrm{sp}} \frac{\left(d_0 + \frac{2x}{\rho_m A_{n-1}}\right)^2}{d_0^2} \tag{2}$$

In which A_{sp} is the total specific surface area for the current batch of powder (m^2), d_0 is the average diameter (m) of the uncoated particles, and ρ_m is the molar density (mol/m^3). A NH_3 dose of 300 s at a rate of 1 sccm equals 1.3 mmol of NH_3, which means that, if all NH_3 is used, a maximum TiN growth rate of 1.3 mmol per cycle can be achieved [x in Eq. (2)]. The resulting maximum growth per cycle in Ångstroms is given in Fig. 4 (dotted line). The calculated GPC shows a similar decay with increasing number of cycles as the experimentally determined GPC, which confirms that under-dosing is indeed a possible explanation for the decrease in GPC. However, since only 16 and 50 % of the admitted TMDAT and NH_3 shows up in the deposited shells, respectively, it seems unlikely that the observed decrease in GPC is caused by under-dosing.

A third reason is that the reduced growth rate can be found in improper fluidization of the particles. When the particle bed is not properly fluidized, gas can by-pass the particle beds, limiting the chances of contact between precursor molecules and particles. The fluidization of particles is influenced by their density, diameter, and the Van der Waals forces between the particle agglomerates. The presence of a conducting TiN shell will influence the density and attractive forces of the particles. Because TiN has a higher density than SiO_2, the density of coated particles and agglomerates is also higher, making them more difficult to fluidize. Furthermore, attractive van der Waals forces (F_{vdW}) between particles are material dependent. This dependency is characterized by the Hamaker constant A_H in the equation:

$$F_{\mathrm{vdW}} = \frac{A_H R}{12a^2} \tag{3}$$

in which R is the sphere radius and a the separation between the particles. The theoretical Hamaker constant of TiN is approximately 2–3 times higher than that of SiO_2. (Eichenlaub et al. 2002) This means that the attractive forces will increase during TiN deposition, which will negatively influence the ability of the powders to be properly fluidized. (Visser 1989) This will reduce the exposure of the particles to TDMAT.

It should be noted here that the exact specific surface area of the batch is unknown and that such measurements would be unreliable due to the rapid oxidation of the particles and the concomitant increase in shell thickness, particle diameter, and specific area. Analysis of reactor effluent composition by, e.g., mass spectrometry should provide more clear insight in the causes of the low efficiency and decline in GPC (King et al. 2007). This technique was, however, not available to us during this study.

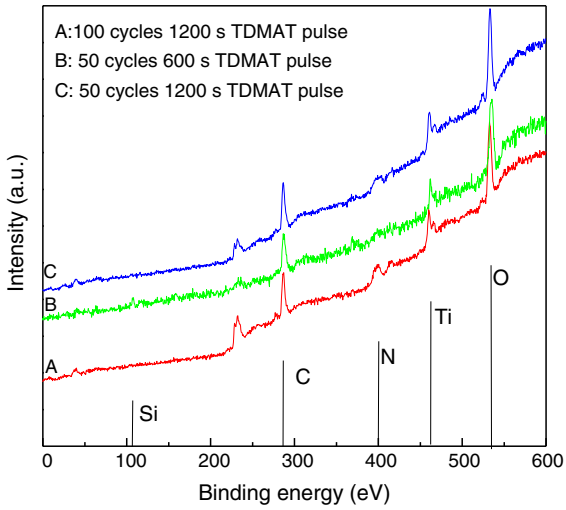

Fig. 5 XPS analysis of three different core–shell powders produced under different circumstances. The letters *A*, *B*, and *C* in the graph correspond to that in Table 2. The *curves* are offset for clarity

Shell composition and structure

Three TiN-coated powders, prepared with varying number of ALD cycles and precursor pulse lengths, were removed from the reactor and analyzed with XPS. The results of the XPS analysis, presented in Fig. 5, show that all powders contain Ti and N. This provides compelling evidence that some form of titanium nitride has been deposited. At the same time, the strong O signal indicates that, at least part of, the TiN shells were oxidized. This probably occurred when opening the reactor and during transport from the reactor to the XPS system.

The unavoidable oxidation of the TiN shell makes it impossible to confirm whether the deposited phase is TiN, Ti_3N_4, or TiO_xN_y. However, oxide formation during the deposition reaction is highly unlikely because the lack of oxygen-containing compounds during reaction.

Integration of the XPS peaks with dedicated software shows that the surface of the particles in certain cases contain traces of Si (<8.8 atom % for sample B, green curve). This is tentatively attributed to the fact that the penetration depth of the XPS signal (~3 nm) may slightly exceed the film thickness. However, we cannot rule out the possibility that the shells are not completely closed, so that some of the underlying SiO_2 is still exposed.

The homogeneity of the shells was investigated with TEM. The bright-field TEM image of particles treated with 100 ALD cycles given in Fig. 6a shows a well-defined core–shell structure for all particles. The shell thickness is highly homogeneous and has a value of approximately 4–5 nm, which is higher than the value estimated from the TiN mass fraction of the powder. This difference is most likely due to the (partial) oxidation of the TiN film, or to the fact that the TiN films are not fully dense. Figure 6b–d depict the elemental distribution of O, Ti, and N, respectively, for the particles. The higher Ti signals at the edges of the particle silhouettes in figure (c) prove that Ti abundance is indeed higher in the surface layer of the particles. The N distribution shows that the concentration of N-atoms is not homogeneously distributed over the different particles. Furthermore, the overall concentration of N-atoms seems much

Table 2 Overview of sample preparation conditions and atomic fractions according to the analysis of the XPS results

Powder	A	B	C
Cycles	100	100	100
NH_3 flow	1	1	1
TDMAT pulse time (s)	1200	600	1200
Weight fraction TiN[a]	0.32	0.24	0.29
Atomic comp. (%) (peak area)			
C1s	46.9 (24,592)	45.7 (15,730)	47.2 (27,676)
N1s TiN	8 (7043)	3.6 (2091)	6.9 (6766)
O1s SiO2	35.8 (46,112)	38.8 (32,820)	38 (54,744)
Si2s SiO2	3.2 (1744)	8.8 (3106)	3.2 (1907)
Ti2p TiO2	6.1 (22,274)	3.1 (7462)	4.8 (19,855)
Ratio Si/Ti	0.5	2.8	0.7
Ratio N/Ti	1.3	1.2	1.4

The numbers in brackets give the peak area in the XPS measurements

[a] Before contact with air

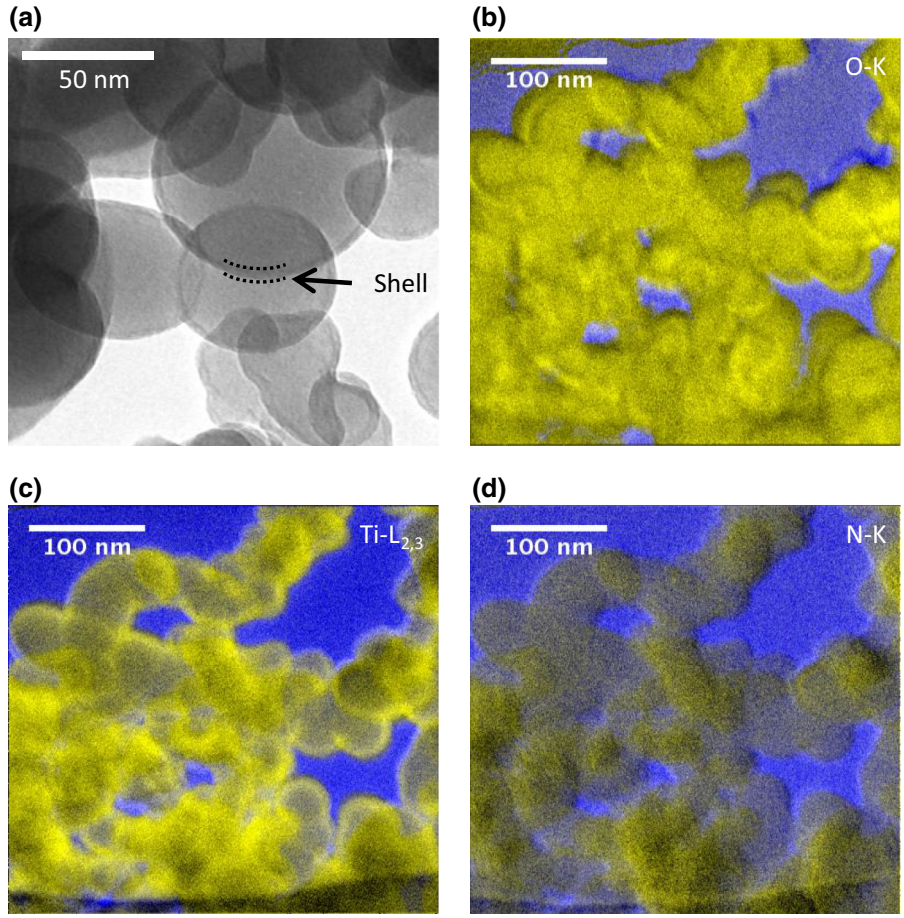

Fig. 6 **a** zero-loss filtered TEM bright-field images of SiO_2–TiO_2 nanoparticles after 100 cycles ALD clearly showing the core–shell structure. Images **b**, **c**, and **d** show the O, Ti, and N distributions, respectively, as obtained by elemental mapping. The light (*yellow*) *dots* indicate presence of O, Ti, and N. (Color figure online)

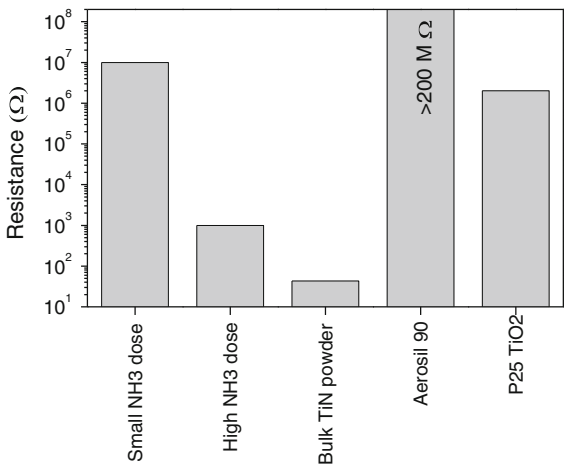

Fig. 7 Resistance of core–shell powder synthesized with a small and a high NH_3 dose and control samples of pure TiN, uncoated Aerosil powder, and P25 TiO_2

lower than the Ti concentration. The O distribution (Fig. 6b) is quite homogeneous over the particle, and the shells are not clearly visible. This confirms that the indeed the Ti on the shell was oxidized. This is in agreement with the XPS analysis and is attributed to (partial) oxidation of the TiN upon exposure to air.

Shell conductivity

To verify that the TiN coating is conductive, the electrical resistance of small amounts (approximately 10 mg) of powder pressed between two 45 mm^2 conducting glass (FTO) electrodes was measured and compared to control samples. The results given in Fig. 7 show that a resistance of 10 MΩ was measured for particles produced with a NH_3 dose of

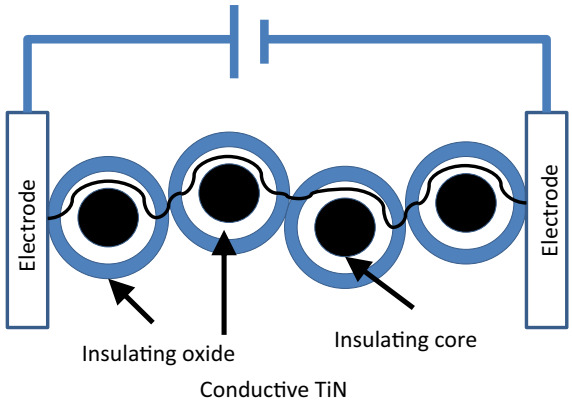

Fig. 8 Illustration of an electron path through a layer of core–shell particles

300 s per cycle at 1 sccm, whereas 300 s flow at 3 sccm resulted in a resistance of 1 kΩ.

For comparison, the resistances of commercial TiN, SiO_2, and TiO_2 powders were measured as well. The commercial TiN powder has a negligible resistance; the measured value of 40 Ω is due to the resistance of the FTO glass. This is consistent with small bulk resistivity of TiN (typically less than 100 μΩ cm) from which a powder resistance of <1 Ω is expected. The resistance of the Aerosil powder is beyond the measuring range of the multimeter (200 MΩ), whereas P-25 TiO_2 has a resistance of 2 MΩ. These results clearly show that the TiN shell, even after being partially oxidized, greatly improves the overall conductivity of the SiO_2 powder.

Assuming a powder fill fraction of ~30 % and a TiN volume fraction in the particles of approximately 45 % (assuming a 2.6 nm shell of pure TiN on a 25 nm particle) an apparent TiN resistivity of 11 kΩ cm is calculated using the equation $\rho = RA\varepsilon V_{\mathrm{TiN}}/L$, in which ε is the volume fraction of powder (−), V_{TiN} is the assumed volume fraction TiN in the powder (−), A is the area of the measurement electrodes (0.45 cm^2), and L is the length between the two measurement electrodes (0.005 cm). The measured resistivity of the layer of core–shell particles is thus several orders of magnitude higher than that of bulk TiN, for which the resistivity typically is less than 100 μΩ cm and ALD-TiN, for which the resistivity is typically in the order of mΩ cm–Ω cm. (Elam et al. 2003; Elers et al. 2005; Kim 2003; Langereis et al. 2006; Musschoot et al. 2009) The much larger resistance can be caused by different factors. First of all, the resistivity of ALD-TiN depends strongly on the deposition conditions: deposition temperature, NH_3 exposure, and use of plasma-enhanced ALD influence the film structure and impurity concentration in the film (Elam et al. 2003; Elers et al. 2005; Langereis et al. 2006). Earlier work on thermal and plasma-enhanced TiN deposition on nanoparticles even showed that the resistivity of TiN coatings deposited with thermal ALD was so large, it could not be measured (Longrie et al. 2014b). The influence of deposition conditions is also demonstrated in this work by the difference in resistance between the sample with a small and large NH_3 dose. Furthermore, the resistivity of thin TiN films varies strongly with film thickness and is seen to increase sharply at thicknesses smaller than 10 nm (as measured with in situ ellipsometry during ALD) (Langereis et al. 2006) or even below 50 nm (measured ex situ with four-point probe measurements) (Assaud et al. 2014). But the most important factor that increases the resistivity of the films is likely to be the oxidized layer on top of the partially oxidized TiN shell (depicted in Fig. 8). The insulating oxide layer forms a large potential barrier between two particles that will have a large effect on the total resistance of the powder. Furthermore, the presence of uncoated particles could also affect the apparent resistivity of the material, although it is not expected to have the order-of-magnitude influence that is measured here. We did not, however, investigate this in more detail.

Conclusions

We have successfully deposited conductive TiN shells on SiO_2 nanoparticles with fluidized bed atomic layer deposition. The growth saturated at approximately 0.4 Å/cycle after 50 cycles with high TDMAT dosage. The growth rate decreased when the number of cycles increased. The particles have the desired core–shell structure and XPS measurements confirm that we indeed have deposited a coating containing Ti and N. However, exposure of the TiN-SiO_2 core–shell nanoparticles to air rapidly oxidizes the TiN to TiO_xN_y, which prevented unequivocal identification of the deposited TiN phase. The (partially oxidized) TiN shells are electrically conducting with an apparent resistivity of >10 kΩ cm. This resistivity is much

higher than expected for pure TiN shells, which is attributed to the (partial) oxidation of TiN.

Acknowledgments The authors would like to thank Jeroen van de Waterbeemd for his help in the experimental work, and Ruud van Ommen (Delft University of Technology), Diana Nanu (Thin Film Factory B.V.), and Wim Besling (NXP) for stimulating discussions. This research is financially supported by the Thin Film Nanomanufacturing program of the Dutch Technology Foundation STW (project 10016).

Appendix

The mass fraction x is defined as the ratio of the shell mass and the total mass of the core–shell particle.

$$x_{\mathrm{TiN}} \equiv \frac{m_{\mathrm{shell}}}{m_{\mathrm{shell}} + m_{\mathrm{core}}}. \tag{4}$$

The mass of the core is equal to

$$m_{\mathrm{core}} = \rho_{\mathrm{SiO_2}} \frac{\pi}{6} d_{\mathrm{core}}^3. \tag{5}$$

The mass of the shell is equal to

$$m_{\mathrm{shell}} = \rho_{\mathrm{TiN}} \frac{\pi}{6} \left((d_{\mathrm{core}} + 2d_{\mathrm{shell}})^3 - d_{\mathrm{core}}^3 \right). \tag{6}$$

Using Eq. (5) and (6) into (4) yields

$$x_{\mathrm{TiN}} = \frac{\left((d_{\mathrm{core}} + 2d_{\mathrm{shell}})^3 - d_{\mathrm{core}}^3 \right)}{\left((d_{\mathrm{core}} + 2d_{\mathrm{shell}})^3 - d_{\mathrm{core}}^3 \right) + \frac{\rho_{\mathrm{SiO_2}}}{\rho_{\mathrm{TiN}}} d_{\mathrm{core}}^3}. \tag{7}$$

Rewriting this equation yields

$$d_{\mathrm{shell}} = \frac{d_{\mathrm{core}}}{2} \left(\sqrt[3]{\frac{x}{1-x} \frac{\rho_{\mathrm{SiO_2}}}{\rho_{\mathrm{TiN}}} + 1} - 1 \right). \tag{8}$$

Assuming a constant growth rate (*GPC*) one can relate the shell thickness to the amount of cycles N.

$$d_{\mathrm{shell}} = N \times \mathrm{GPC}. \tag{9}$$

This results in

$$\mathrm{GPC} = \frac{d_{\mathrm{core}}}{2N} \left(\sqrt[3]{\frac{x}{1-x} \frac{\rho_{\mathrm{SiO_2}}}{\rho_{\mathrm{TiN}}} + 1} - 1 \right). \tag{10}$$

References

Amarnath CA, Nanda SS, Papaefthymiou GC, Yi DK, Paik U (2013) Nanohybridization of low-dimensional nanomaterials: synthesis, classification, and application. Crit Rev Solid State Mater Sci 38:1–56. doi:10.1080/10408436.2012.732545

Assaud L, Pitzschel K, Hanbucken M, Santinacci L (2014) Highly-conformal TiN thin films grown by thermaland plasma-enhanced atomic layer deposition. ECS J Solid State Sci Technol 3:253–258

Boriskina SV, Ghasemi H, Chen G (2013) Plasmonic materials for energy: From physics to applications. Mater Today 16:375–386. doi:10.1016/j.mattod.2013.09.003

Cortie MB, Giddings J, Dowd A (2010) Optical properties and plasmon resonances of titanium nitride nanostructures. Nanotechnology 21:115201

Didden AP, Middelkoop J, Besling WFA, Nanu DE, van de Krol R (2014) Fluidized bed atomic layer deposition reactor for the synthesis of core-shell nanoparticles. Rev Sci Instrum 85:013905

Eichenlaub S, Chan C, Beaudoin SP (2002) Hamaker constants in integrated circuit metalization. J Colloid Interface Sci 248:389–397. doi:10.1006/jcis.2002.8241

Elam JW, Schuisky M, Ferguson JD, George SM (2003) Surface chemistry and film growth during TiN atomic layer deposition using TDMAT and NH_3. Thin Solid Films 436:145–156

Elers KE et al (2002) Diffusion barrier deposition on a copper surface by atomic layer deposition. Chem Vap Depos 8:149–153. doi:10.1002/1521-3862(20020704)8:4<149:aid-cvde149>3.0.co;2-f

Elers K-E, Winkler J, Weeks K, Marcus S (2005) TiCl4 as a precursor in the TiN deposition by ALD and PEALD. J Electrochem Soc 152:G589–G593. doi:10.1149/1.1938108

Fillot F et al (2005) Investigations of titanium nitride as metal gate material, elaborated by metal organic atomic layer deposition using TDMAT and NH_3. Microelectron Eng 82:248–253

Grillo F, Kreutzer MT, van Ommen JR (2015) Modeling the precursor utilization in atomic layer deposition on nanostructured materials in fluidized bed reactors. Chem Eng J 268:384–398. doi:10.1016/j.cej.2015.01.067

Hakim LF, Blackson J, George SM, Weimer AW (2005a) Nanocoating individual silica nanoparticles by atomic layer deposition in a fluidized bed reactor. Chem Vap Depos 11:420–425

Hakim LF, George SM, Weimer AW (2005b) Conformal nanocoating of zirconia nanoparticles by atomic layer deposition in a fluidized bed reactor. Nanotechnology 16:S375–S381

Hakim LF, Portman JL, Casper MD, Weimer AW (2005c) Aggregation behavior of nanoparticles in fluidized beds. Powder Technol 160:149–160. doi:10.1016/j.powtec.2005.08.019

Hayes HM, Lide DR (2015) CRC handbook of chemistry and physics. CRC Press, Boca Raton

Heil T, Kohl H (2010) Optimization of EFTEM image acquisition by using elastically filtered images for drift correction. Ultramicroscopy 110:745–750. doi:10.1016/j.ultramic.2010.03.011

Khurshid H et al (2013) Core/shell structured iron/iron-oxide nanoparticles as excellent MRI contrast enhancement agents. J Magn Magn Mater 331:17–20. doi:10.1016/j.jmmm.2012.10.049

Kim H (2003) Atomic layer deposition of metal and nitride thin films: current research efforts and applications for semiconductor device processing. J Vac Sci Technol B 21:2231–2261. doi:10.1116/1.1622676

King DM, Spencer JA, Liang X, Hakim LF, Weimer AW (2007) Atomic layer deposition on particles using a fluidized bed reactor with in situ mass spectrometry. Surf Coat Technol 201:9163–9171

Langereis E, Heil SBS, van de Sanden MCM, Kessels WMM (2006) In situ spectroscopic ellipsometry study on the growth of ultrathin TiN films by plasma-assisted atomic layer deposition. J Appl Phys 100:10. doi:10.1063/1.2214438

Logothetidis S, Meletis EI, Stergioudis G, Adjaottor AA (1999) Room temperature oxidation behavior of TiN thin films. Thin Solid Films 338:304–313. doi:10.1016/S0040-6090(98)00975-4

Longrie D, Deduytsche D, Detavernier C (2014a) Reactor concepts for atomic layer deposition on agitated particles: a review. J Vac Sci Technol A 32:010802. doi:10.1116/1.4851676

Longrie D, Deduytsche D, Haemers J, Smet PF, Driesen K, Detavernier C (2014b) Thermal and plasma-enhanced atomic layer deposition of TiN using TDMAT and NH_3 on Particles agitated in a rotary reactor. ACS Appl Mater Interfaces 6:7316–7324. doi:10.1021/am5007222

Ma N, Marshall AF, Gambhir SS, Rao JH (2010) Facile synthesis silanization, and biodistribution of biocompatible quantum dots. Small 6:1520–1528. doi:10.1002/smll.200902409

Magdassi S, Grouchko M, Kamyshny A (2010) Copper nanoparticles for printed electronics: routes towards achieving oxidation stability. Materials 3:4626–4638. doi:10.3390/ma3094626

Miikkulainen V, Leskela M, Ritala M, Puurunen RL (2013) Crystallinity of inorganic films grown by atomic layer deposition: overview and general trends. J Appl Phys 113:021301

Musschoot J, Xie Q, Deduytsche D, Van den Berghe S, Van Meirhaeghe RL, Detavernier C (2009) Atomic layer deposition of titanium nitride from TDMAT precursor. Microelectron Eng 86:72–77

Okada LA, George SM (1999) Adsorption and desorption kinetics of tetrakis(dimethylamino)titanium and dimethylamine on TiN surfaces. Appl Surf Sci 137:113–124. doi:10.1016/S0169-4332(98)00375-4

Ren MM, Zhou Z, Gao XP, Peng WX, Wei JP (2008) Core-shell Li3V2(PO4)@C composites as cathodic materials fro lithium-ion batteries. J Phys Chem C 112:5689–5693

Snyder MQ, Trebukhova SA, Ravdel B, Wheeler MC, DiCarlo J, Tripp CP, DeSisto WJ (2007) Synthesis and characterization of atomic layer deposited titanium nitride thin films on lithium titanate spinel powder as a lithium-ion battery anode. J Power Sources 165:379–385. doi:10.1016/j.jpowsour.2006.12.015

Tedsree K et al. (2011) Hydrogen production from formic acid decomposition at room temperature using a Ag–Pd core-shell nanocatalyst. Nat Nanotechnol 6:302–307. http://www.nature.com/nnano/journal/v6/n5/abs/nnano.2011.42.html#supplementary-information

van Ommen JR, Yurteri CU, Ellis N, Kelder EM (2010) Scalable gas-phase processes to create nanostructured particles. Particuology 8:572–577. doi:10.1016/j.partic.2010.07.010

Visser J (1989) Van der Waals and other cohesive forces affecting powder fluidization. Powder Technol 58:1–10. doi:10.1016/0032-5910(89)80001-4

Wank JR, George SM, Weimer AW (2004) Nanocoating individual cohesive boron nitride particles in a fluidized bed by ALD. Powder Technol 142:59–69

Zhang H, Jin M, Xia Y (2012) Enhancing the catalytic and electrocatalytic properties of Pt-based catalysts by forming bimetallic nanocrystals with Pd. Chem Soc Rev 41:8035–8049

Zhao J, Garza EG, Lam K, Jones CM (2000) Comparison study of physical vapor-deposited and chemical vapor-deposited titanium nitride films usng X-ray photoelectron spectroscopy. Appl Surf Sci 158:246–251